



Cite this: DOI: 10.1039/c8nj04314k

Functionalization of gold nanoparticles with two aminoalcohol-based quinoxaline derivatives for targeting phosphoinositide 3-kinases (PI3K α)†

Janine Araújo,^a Fabrício G. Menezes,^a Heloiza F. O. Silva,^a Davi S. Vieira,^a Sergio R. B. Silva,^b Adailton J. Bortoluzzi,^c Celso Sant'Anna,^d Mateus Eugenio,^d Jannyely M. Neri^a and Luiz H. S. Gasparotto^b*^a

Quinoxaline derivatives have attracted considerable attention due to their vast range of applications that includes electroluminescence and biomedicine. Concerning the latter, the literature has shown that compounds with a quinoxaline motif bind quite efficiently to phosphatidylinositol-4,5-bisphosphate 3-kinases (PI3Ks), which are enzymes found to be overexpressed in some types of neoplasms. In the present study, gold nanoparticles (AuNPs) were easily functionalized with 2,3-dihydro-1,4-oxazino[2,3-*b*]quinoxalin-4-yl)ethanol (DEQX) and 2-(2,3-dihydro-1,4-oxazino[2,3-*b*]quinoxalin-4-yl)ethanol (OAQX). We made use of glycerol in alkaline media as reducing agent and the quinoxalines served as capping ligands to stabilize the AuNPs. This is the first report on the modification of a nanostructure with quinoxalines. Functionalization confers nanoparticles the required specificity to target only cancer cells, which opens possibilities for phototherapy since the modified AuNPs would concentrate in the tumor tissue as a consequence of PI3K α overexpression. Molecular dynamics simulations have shown that DEQX and OAQX are potential inhibitors of PI3K α since they bind to the active site of the enzyme in a way similar to other known inhibitors.

Received 23rd August 2018,
Accepted 16th December 2018

DOI: 10.1039/c8nj04314k

rsc.li/njc

1 Introduction

Cancer is a multiple-factor malady caused by accumulation of genetic mutations that lead to abnormal proliferation of tissues. An important consequence of decoding the human genome sequence was the facilitation of the analysis of cancer genomes.¹ This advance was of paramount importance for locating the most frequently mutated genes that are directly correlated to overexpressed proteins upon tumor growth.² As examples, there are E-cadherin and β -catenin, which are proteins that play important roles in cell-cell adhesion and whose overexpression is associated with colorectal carcinomas.^{3,4} In the case of brain tumor, atypical augmentation of phosphatidylinositol-4,5-bisphosphate 3-kinases (PI3Ks)

has been implicated in that severe type of neoplasm.^{5,6} The clarification of the molecular mechanism of cancer signaling allowed the development of pharmacological inhibitors that target specific proteins to halt or cease tumor cell progression.⁷ As an example, monoclonal antibodies have been considerably successful for cancer therapy in recent years,⁸ as they can be precisely engineered to fit a specific protein's active site in order to inhibit its action. However, the production of monoclonal antibodies is a laborious and time-consuming technology.⁹ An interesting approach to circumvent these features is the design of molecules that have high affinity to the desired protein's site and are easily synthesized through simple routes.¹⁰ Quinoxaline derivatives have attracted considerable attention due to their vast range of applications that includes luminescence¹¹ and biomedicine.¹² Concerning the latter, compounds with a quinoxaline motif are quite efficient antitumor¹³ and anticancer agents^{14,15} as they inhibit enzymes involved in cancer proliferation, motility and differentiation. Mielcke *et al.*¹⁶ found that quinoxaline-derived calchones were able to inhibit glioma cell proliferation through binding with the PI3K enzyme. The PI3K α enzyme, which is a subclass of PI3Ks, is regarded as potential therapeutic target due its role in several types of cancer.^{17,18} In this context, Wu *et al.*^{19,20} reported the design and synthesis of a series of biologically active 2,3-disubstituted quinoxaline derivatives and also made use of computational

^a Biological Chemistry and Chemometrics Research Group, Institute of Chemistry, Federal University of Rio Grande do Norte, Lagoa Nova, 59072-970, Natal, RN, Brazil. E-mail: lhgasparotto@ufrnet.br; Tel: +55 84 3342 2323

^b Brain Institute, Federal University of Rio Grande do Norte, Morro Branco, 59056-450, Natal, RN, Brazil

^c Laboratório de Bioinorgânica e Cristalografia, Departamento de Química, Universidade Federal de Santa Catarina, 88040-900 Florianópolis-SC, Brazil

^d Laboratory of Microscopy Applied to Life Science – Lamav, National Instituto of Metrology, Quality and Technology – Inmetro, Duque de Caxias, 25250-020, Rio de Janeiro, RJ, Brazil

† Electronic supplementary information (ESI) available. See DOI: 10.1039/c8nj04314k

chemistry to suggest binding modes between the PI3K α active site and the quinoxaline derivatives.

Nowadays, targeted therapies may be substantially enhanced by bringing nanotechnology to the field, as it has been employed successfully in imaging,^{21,22} diagnosing²³ and cancer treatment.²⁴ However, nanomaterials usually lack specificity and must be previously functionalized in order to become a task-specific hybrid.²⁵ In particular, the surface of gold nanoparticles (AuNPs) may be modified with a variety of compounds such as proteins, DNA, and antibodies,²⁶ to confer them the specificity required for targeted therapies.

Herein, the functionalization and stabilization of AuNPs with two synthetic quinoxaline derivatives, 2,3-diethanolminoquinoxaline (DEQX) and 2-(2,3-dihydro-[1,4]oxazino[2,3-*b*]quinoxalin-4-yl)ethanol (OAQX) were described. To the best of our knowledge, this is the first study on the functionalization of AuNPs with quinoxaline-based molecules. Another point worth mentioning is that, despite the low solubility of heterocyclic units in water, we were able to functionalize the gold nanoparticles with both quinoxaline-based molecules in aqueous solution, which is quite an important aspect for medicinal purposes.²⁷ Computational studies suggested good affinity to the active site of the PI3K α . In this way, based on these preliminary results, the quinoxaline-AuNPs conjugates are envisaged as dual-function hybrid units that (i) may prevent the proliferation of tumor cells that are dependent on the PI3K α enzyme and (ii) could be suitable for cancer phototherapy since the modified AuNPs concentrates in the tumor tissue as a consequence of the PI3K α overexpression.

2 Experimental section

2.1 Computational methodology

The association of DEQX and OAQX with the PI3K α binding site was first studied *via* docking using the Autodock Vina software.²⁸ The tridimensional structure of PI3K α enzyme was obtained from a 2.8 Å resolution X-ray structure (PDB entry 3HHM).²⁹ The structure of PI3K α enzyme was prepared for docking with AutoDockTools 1.5.6 (ADT).³⁰ The three-dimensional structures of DEQX and OAQX were built with Avogadro software.³¹ A 25 × 30 × 30 Å³ grid was centered near the center of the binding pocket, and the exhaustiveness parameter was set to 32.

Molecular dynamics (MD) simulations were then performed with the structures from docking procedures. The minimum distance of the quinoxaline-PI3K α complex to the box wall was at least 12 Å, hence the dimensions of the simulation box were chosen accordingly. The systems were neutralized with sodium and chloride ions until reaching the concentration of 0.15 mol L⁻¹. The AMBER ff03 force field³² was employed with the with the GROMACS 5.0 software package. The topology and parameters for the ligands were generated with the General Amber Force Fields with structure and charges calculated using HF/6-31G(d) as the level of theory and RESP fit.³³ All quantum mechanics calculations were performed using GAMESS. MD simulations were carried out at neutral pH in NVT ensemble at a temperature of 310 K controlled by the V-rescale thermostat algorithm.³⁴

Covalent bonds involving hydrogen were restrained by LINCS algorithm³⁵ while SPC water molecules geometries were constrained by the SETTLE³⁶ algorithm. Motion equations were integrated by a leap-frog³⁷ algorithm with time steps of 2.0 fs. The long-range interactions were computed using particle-mesh Ewald sum, PME,³⁸ with a cutoff of 10 Å also used for van der Waals interactions. An energy minimization step using steepest descent³⁹ was employed before the equilibration phase. The properties related with structural dynamics were monitored by root-mean-square deviations (RMSD) using C α atoms and the initial structure of the simulation ($t = 0$ ns) as reference structure. The hydrogen bonds (HB) between amino acids residues and ligands were identified based on geometric criteria, the distance between acceptor and donor < 3.5 Å, and the angle donor-hydrogen-acceptor < 30°. ⁴⁰ The interaction potential energy (IPE) for ligand-residue and ligand-water molecules can be computed according to $\sum_i^{N_i} \sum_j^{N_j} E_{ij}$, where E_{ij}

is the interaction energy between a group of atoms from ligand (i) and a group of atoms from residue j , and N_i and N_j are the total number of atoms on molecules/residues i and j , respectively. The cutoff for this calculation was set to 6 Å from each ligand.

Surface electrostatic potentials were generated using the USCF Chimera software with Adaptive Poisson-Boltzmann Solver (APBS) interface⁴¹ and the images were produced by VMD visualization software.⁴²

2.2 Materials and instrumentation

All chemicals were purchased from commercial sources (Sigma-Aldrich and Tedia) and used without further purification. Melting points were measured in a Microquímica MQAPF-301 and the values were not corrected. Elemental analysis of carbon, hydrogen and oxygen was performed in a Carlo Erba E-110 instrument. UV-vis analyses were carried out with an Evolution 60S UV-visible spectrophotometer (Thermo Scientific). Infrared spectra were acquired in a 283 Perkin-Elmer instrument. Nuclear magnetic resonance (NMR) analyses were conducted in a Varian Mercury Plus-400 MHz. Transmission electron microscopy (TEM) images were acquired with a FEI Tecnai G² Spirit BioTWIN microscope operating at 120 kV.

2.3 Synthesis and spectroscopic characterization of DEQX and OAQX

2.3.1 2,3-Dichloroquinoxaline (DCQX). This starting material was prepared by a two-step protocol according to.⁴³ The protocol involves the acid catalyzed cyclization of *o*-phenylenediamine and oxalic acid to generate 1,4-dihydroquinoxaline-2,3-dione, which reacts with thionyl chloride to afford the starting material DCQX at 79% yield.

2.3.2 2,3-Diethanolminoquinoxaline (DEQX). A solution of DCQX (0.50 g, 2.5 mmol) in ethanolamine (5 ml) was kept at 100 °C for three hours. Afterwards, 25 ml of cold water were added and the final aqueous solution was maintained in ice bath for 8 h. The resulting solid was filtered and recrystallized from water to give the pure compound.

Mp 179 °C (Lit. 175–177 °C⁴⁴). IR (KBr) ν_{\max} (cm⁻¹): 3413, 3199, 2974, 2921, 1555, 1514, 1465, 1047, 765. ¹H NMR (400 MHz, CDCl₃) δ (ppm) 7.38 (m, 2H), 7.15 (m, 2H), 7.03 (t, *J* = 5.0 Hz), 4.83 (t, *J* = 5.4 Hz), 3.66 (m, 4H), 3.56 (m, 4H). ¹³C NMR (100 MHz, DMSO-D₆) δ (ppm) 143.8, 136.4, 124.5, 123.2, 59.4, 43.6. Elemental analysis for C₁₂H₁₆N₄O₂: C, 58.05; H, 6.50; N, 22.57; found: C, 58.12; H, 6.63; N, 22.68. Yield: 85%.

2.3.3 2-(2,3-Dihydro-[1,4]oxazino[2,3-*b*]quinoxalin-4-yl)ethanol (OAQX). Prepared similarly to DETQ, except by the use of diethanolamine instead ethanolamine.

Mp 160 °C (Lit. 159–161 °C⁴⁵). IR (KBr) ν_{\max} (cm⁻¹): 3284, 2992, 2862, 1658, 1566, 1456, 1342, 1058, 771. ¹H NMR (400 MHz, CDCl₃) δ (ppm) 7.54–7.51 (m, 2H), 7.40–7.37 (m, 1H), 7.29–2.26 (m, 1H), 4.83 (t, *J* = 5.2 Hz, 1H), 4.47–4.45 (m, 2H), 3.77–3.71 (m, 6H). ¹³C NMR (100 MHz, DMSO-D₆) δ (ppm) 147.6, 142.8, 139.2, 134.9, 127.7, 126.1, 124.7, 123.8, 64.3, 60.0, 49.9, 46.1. Elemental analysis for C₁₂H₁₃N₃O₂: C, 62.33; H, 5.67; N, 18.17; found: C, 62.40; H, 5.80; N, 18.26. Yield: 81%.

2.4 Preparation of quinoxaline-functionalized AuNPs

AuNPs were prepared through a previously reported method^{46,47} that was slightly modified in this study. In the method, glycerol in alkaline medium is used as reducing agent and the modification consisted in replacing polyvinylpyrrolidone (the stabilizing agent) with the quinoxalines synthesized in this work. The concentrations of gold ions, glycerol and NaOH were kept at 0.5 mmol L⁻¹, 0.10 mol L⁻¹ and 0.10 mol L⁻¹, respectively. The amounts of DEQX and OAQX varied as such to generate the following Au³⁺/quinoxaline molar ratios: 1:1, 1:0.5, 1:0.2, 1:0.1, 1:0.05, 1:0.01, and 1:0.005. The reaction was carried out by adding a 5 mL solution of glycerol + NaOH into another 5 mL solution that contained Au³⁺ and a quinoxaline. The final mixtures had red-to-violet colors characteristic of gold nanoparticles.

3 Results and discussion

3.1 Molecular modeling

PI3K α are well established enzymes as promising targets for cancer therapy in humans. Small molecules based on quinoxaline moiety have their anti-tumor activity hypothesized in terms of binding to P3K α .¹⁹ It is suggested that hydrogen bonds between oxygen atoms of amine moieties and Val851 and Ser854 residues are crucial to the activity, with some other possible interactions involving arylsulfonyl units. The present investigation provides an analysis initially based on molecular docking models between PI3K α enzyme and DEQX and OAQX molecules and then the best structures from docking were used for MD simulations. Since host–guest intermolecular interactions could be a primary condition for a successfully structure-based drug design, we have analyzed the binding site of the receptor by interaction potential energy (IPE) from MD simulations to obtain the individual contribution of each amino acid residue, ranking the most relevant interactions among the molecules.

The 6 Å sphere centered on each quinoxaline molecule was used for the calculation of IPE. Although such a sphere

comprised thirty two neighboring residues, the results revealed that the following twelve interacted with both quinoxalines only slightly, with energies no lower than -0.1 kcal mol⁻¹: Ile771, Leu779, Glu798, Leu807, Asp810, Leu814, Gly837, Cys838, Ser919, Lys924, His931, and Asp933. The other twenty residues are listed in Fig. 1A with their respective IPE for both quinoxalines. Considering an arbitrary cutoff of -1.0 kcal mol⁻¹, only six residues (Ile932, Met922, Ser854, Val851, Ile800, Met772) are hotspots for both quinoxalines. Gln859, Val850, Ser773 are hotspots for DEQX, while Asn853 and Trp780 are hotspots for OAQX. On the other hand, nine residues (Phe930, Thr856, His855, Arg852, Glu849, Ile848, Tyr836, Ser774 and Pro778) interact with neither quinoxalines. Fig. 1B and C present a visualization of the local structure of the hotspots for (A) DEQX and (B) OAQX.

Val851 and Ser854 deserve further attention due to their high quinoxaline-P3K α IPE (Fig. 1A). In the case of Val851, the more attractive IPE is due to the hydrogen bond between its amide backbone moiety and the hydroxyl group of the quinoxalines. This type of interaction is reported to be crucial to kinase-inhibitor complexes.^{48,49} Similarly, the Ser854 residue has an amide backbone and a side-chain hydroxyl conferring it high potential to form hydrogen bonds with ligands.¹⁹ The short distance of these hydrogen bonds, (around 2.22 Å and 2.05 Å for DEQX and OAQX, respectively) and the high occurrence frequency (100% and around 89.5% for DEQX and OAQX, respectively) strongly suggests that the Ser854 is also a key residue for the specific inhibition process. In both cases, the intermolecular hydrogen bonds are also favored by the flexibility of 2-hydroxyethyl group ($-\text{CH}_2\text{CH}_2\text{OH}$) of DEQX and OAQX, respectively.

Although Ile932 is not as energetic as Val851 and Ser854, it qualifies as a hotspot due to its non polar nature that allows for hydrophobic interactions with the aromatic ring portion of the quinoxalines. Furthermore, the absence of a Ile932 residue would lead to total loss of enzyme activity.⁴⁹ Val850, Ile848, Ile800, Met922, Phe930, and Ile932 residues are constituents of ATP binding site interacting as hotspots *via* hydrophobic contacts with DEQX and OAQX. The other residues presented in the Fig. 1A play a collaborative role as secondary hotspots. Concerning electrostatic interactions, it is known that they may guide binding processes in biological environments.⁴¹ In Fig. 1D and E, electrostatic surfaces of the P3K α in the presence of DEQX and OAQX clearly show that the hydroxyl group is highly adaptive in biological environment due to its amphoteric functionality.

MD simulations have shown that DEQX and OAQX are potential inhibitors of PI3K α since they bind to the active site of the enzyme in a way similar to other known inhibitors.^{48–50} The correct protein–ligand binding is designed by long range interactions optimizing hydrogen bonds and charge complementarity. Approximately 67% of the protein–ligand (small organic molecules) complexes have hydrogen bonds mediating recognition through NH (backbone) groups of a residue and oxygen atoms of the ligand.⁵¹

3.2 Synthesis and characterization of the target quinoxalines

Classically, quinoxaline cores and their derivatives are synthesized through reactions of aromatic *o*-diamines and

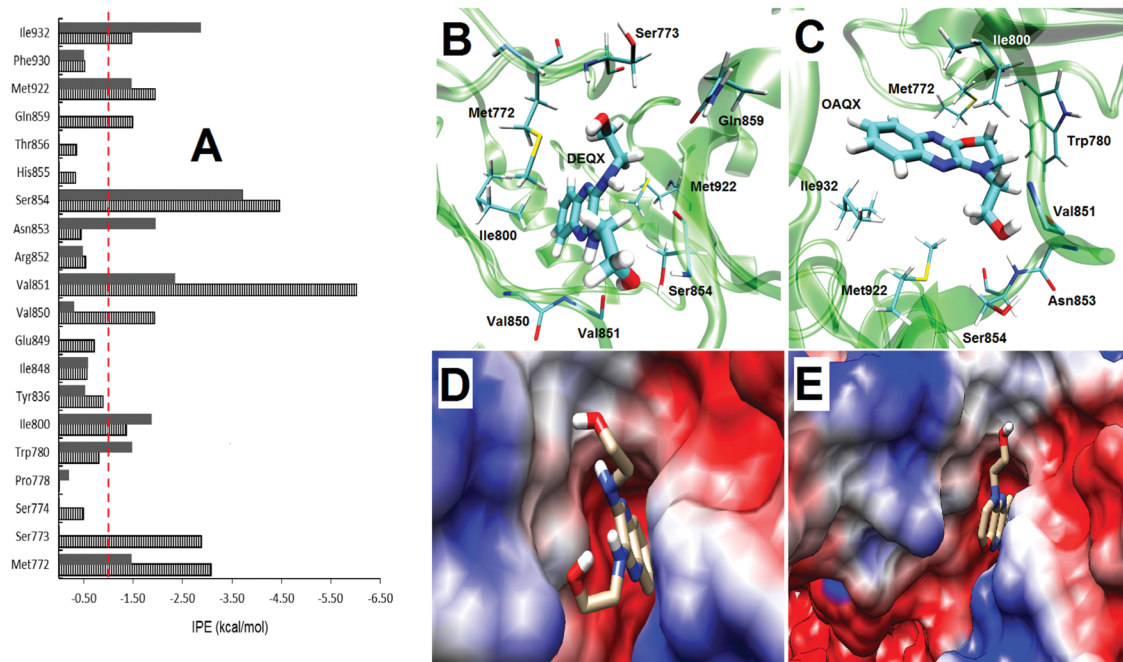


Fig. 1 (A) Interaction potential energy (IPE) for each residue. The values are shown for DEQX (dashed bars) and OAQX (filled bars). The dashed red line indicates the arbitrary limit for the binding process. Structural representation of (B) DEQX and (C) OAQX inside the binding pocket of PI3K α . Water molecules not shown. Electrostatic surface representation of the binding pocket of PI3K α containing (D) DEQX and (E) OAQX.

α -dialdehydes/ α -diketones in the presence of a catalyst.⁵² Other synthetic routes that involve reaction of DCQX with nucleophilic species are also available in literature. The structural features of this substrate allow the generation of innumerable 2- and/or 2,3-substituted quinoxalines, including biologically relevant compounds such as those that present anti-cancer activity due to interactions with PI3K α .^{19,20} In this study, DEQX and OAQX were obtained from reactions of DCQX⁴³ with ethanolamine and diethanolamine, respectively (Fig. 2). DEQX originated from the reaction of DCQX with two equivalents of ethanolamine *via* double *N*-nucleophilic attack, while OAQX was generated by reacting one equivalent of diethanolamine *via* cyclization processes involving simultaneous *N*- and *O*-nucleophilic attacks.

The DEQX and OAQX molecules were fully characterized through elemental analysis, infrared spectroscopy, ¹NMR and ¹³C NMR spectroscopies. Also, OAQX had its structure confirmed by X-ray crystallography (Fig. 2 – inset), as shown in ESI.† Both synthetic quinoxaline derivatives were soluble enough in water to allow the synthesis of AuNPs in aqueous medium.

3.3 Production of DEQX-AuNPs and OAQX-AuNPs

In this study, Au³⁺ ions were reduced by glycerol in alkaline medium at room temperature. As it is biodegradable under aerobic conditions, non-toxic, and relatively inexpensive, glycerol is a “greener” option for generating nanoparticles when compared to common reducing chemicals such as formamide,

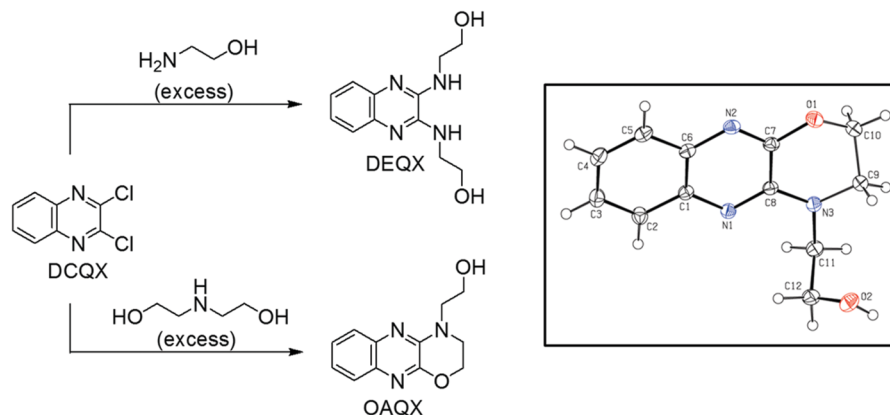


Fig. 2 Synthetic protocol of DEQX and OAQX from DCQX – conditions: ethanolamine or diethanolamine, 100 °C, 3 h. Inset: ORTEP illustration of OAQX determined by X-ray crystallography.

sodium borohydride and hydrazine.⁵³ It is well known that a suitable stabilizing agent is also required in order to control size and aggregation of nanoparticles in solution.⁵⁴ To this end, we investigated the ability of DEQX and OAQX to stabilize gold nanoparticles. In this way, not only would the AuNPs be appropriately available in solution, but they would also be unquestionably functionalized with the quinoxalines employed in this study. Fig. 3 presents UV-vis spectra of AuNPs capped with DEQX (A) and OAQX (B) acquired at different Au³⁺/quinoxaline molar ratios. The Au³⁺ concentration was fixed at 0.50 mmol L⁻¹. Upon increasing the amount of quinoxalines, the UV-vis spectra tended to acquire the shape typically related to spherical AuNPs,⁴⁶ as seen in Fig. 3A and B. The shape of AuNPs will be confirmed later by TEM. The signal observed in the UV-vis experiments reflects the surface plasmon resonance (SPR) of oscillating electrons on the surface of the nanoparticles.⁵⁵ An important difference between DEQX and OAQX is that, comparatively, a much lower concentration of the former is sufficient to generate AuNPs. A DEQX concentration of 25 μmol L⁻¹ (which corresponds to the molar ratio of 1:0.05) is sufficient for the generation of AuNPs, while at least 100 μmol L⁻¹ of OAQX is required for the same purpose. Based on these results, DEQX was more efficient than OAQX for the formation of AuNPs.

Another important feature worth mentioning is the relative amount of AuNPs generated with DEQX and OAQX. In Fig. 3A, the lower absorbance over the Au³⁺/DEQX molar ratio range of 1:0.005–1:0.5 indicates that the amount of nanoparticles

decreased with the augmentation of DEQX concentration. In contrast, the concentration of OAQX impacted only slightly on the amount of AuNPs freshly produced, as evidenced by similar level of absorbances regardless of the Au³⁺/OAQX molar ratio (Fig. 3B). This may be explained by the formation of a relatively stable complex between gold ions and DEQX that competes with the reduction of Au³⁺. In an experiment devised to check on this hypothesis, a Au³⁺ solution was mixed with another of DEQX in absence of glycerol and NaOH and UV-vis spectra were recorded at different times as presented in Fig. 4A. The shoulder at 410 nm that arises with time is attributed to a gradual formation of a yellow-to-orange complex between gold ions and DEQX. Khan *et al.*⁵⁶ reported the formation of a stable yellow-orange complex from the reaction between cetyltrimethylammonium bromide (CTAB) and gold ions. In their study the same shoulder at 410 nm evolved over time upon mixing CTAB with gold ions. Furthermore, a yellow coordination complex has been recently isolated from the reaction of KAuCl₄ and quinoxaline,⁵⁷ which is a further evidence that Au³⁺ is prone to complexation with at least some types of quinoxalines. On the other hand, similar behaviour is not observed for OAQX at the same interval. Upon mixing Au³⁺ with OAQX, a slight intensification of the pale yellow is observed only after 30 min, which might suggest weak complexation to some degree.

It is important to note that after 24 h the absorbance of the DEQX-stabilized AuNPs solutions increased for Au³⁺/DEQX molar ratios between 1:0.05 and 1:0.5 (Fig. 5A), meaning that in the 24 hour interval the Au³⁺-DEQX complex slowly released

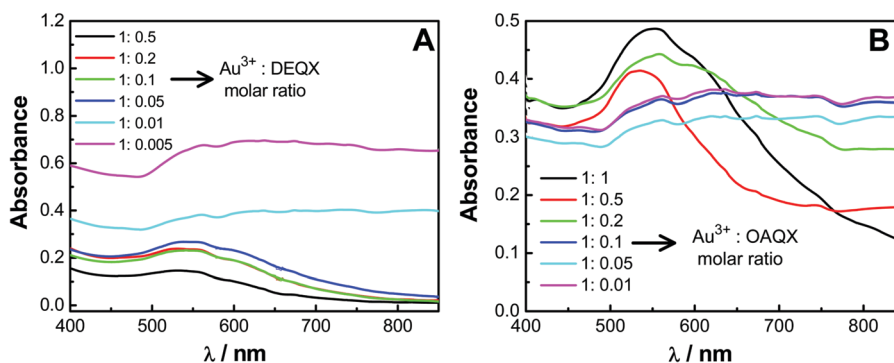


Fig. 3 UV-vis spectra of AuNPs stabilized with (A) DEQX and (B) OAQX at different Au³⁺/quinoxalines molar ratios.

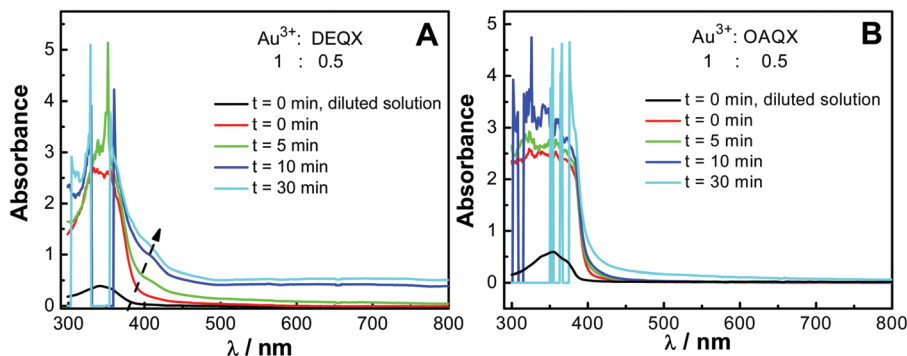


Fig. 4 UV-vis spectra of solutions containing (A) Au³⁺ + DEQX and (B) Au³⁺ + OAQX acquired at different times. Glycerol and NaOH are absent. In both cases the concentrations of Au³⁺ and quinoxalines were 0.50 mmol L⁻¹ and 0.25 mmol L⁻¹, respectively.

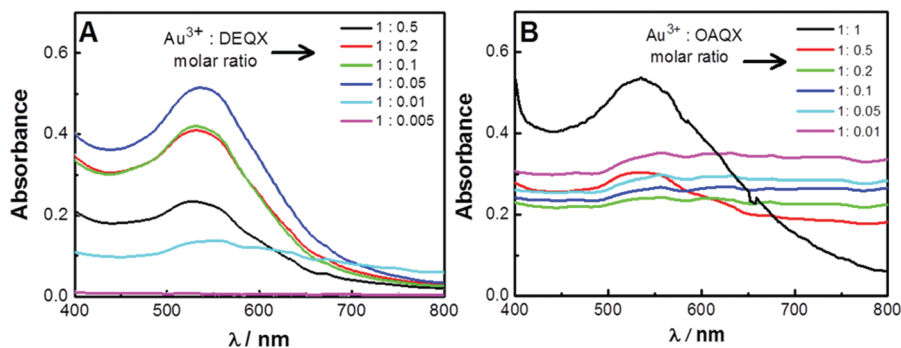


Fig. 5 UV-vis spectra of AuNPs stabilized with (A) DEQX and (B) OAQX at different Au^{3+} /quinoxalines molar ratios. Spectra were acquired 24 h after the synthesis.

gold ions for further formation of AuNPs. Fig. 5A also shows that Au^{3+} /DEQX molar ratios of 1:0.01 and 1:0.005 were not sufficient for stabilization of AuNPs. On the other hand, absorbances from OAQX-capped AuNPs (Fig. 5B) varied only marginally, which corroborates the hypothesis that OAQX binds weakly to Au^{3+} and, therefore, gold ions were promptly available to form

AuNPs. A closer inspection of Fig. 5B reveals that there was a decrease in absorbance for Au^{3+} /OAQX molar ratios other than 1:1, which implies that only in the latter condition stable AuNPs could be obtained with OAQX as capping agent.

Fig. 6 presents TEM images of AuNPs capped with DEQX (A) and OAQX (B) at Au^{3+} /quinoxaline molar ratios of 1:0.2 and

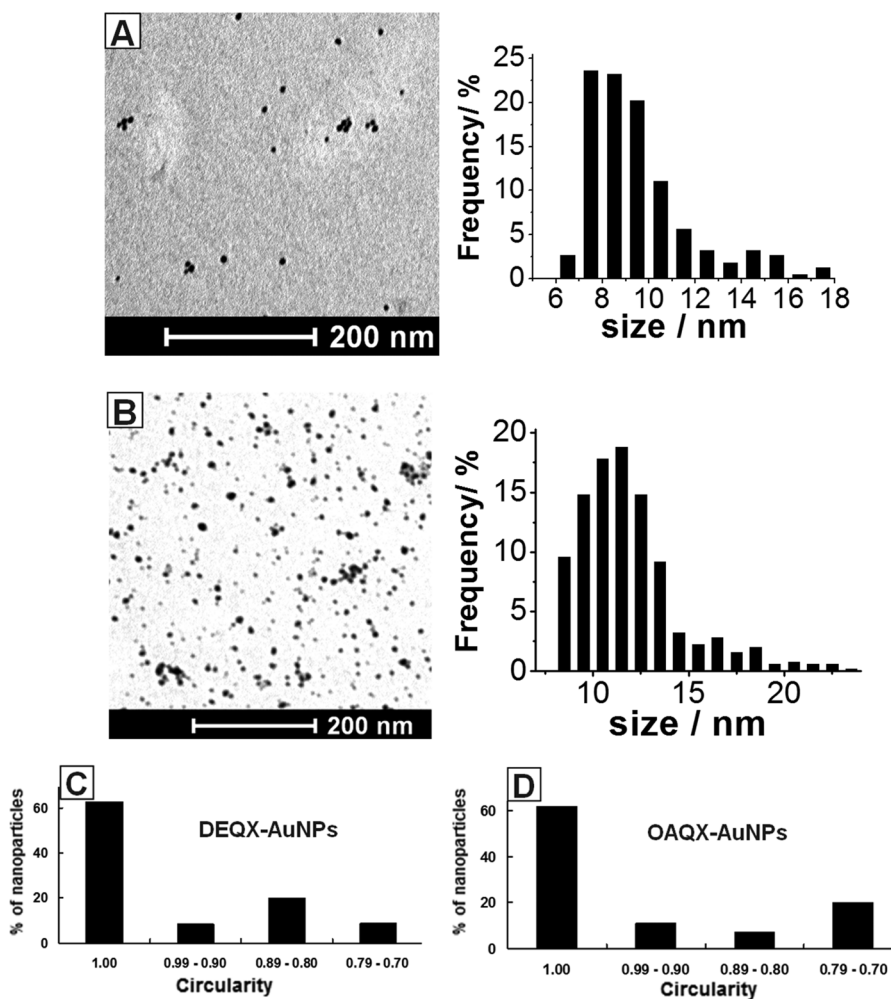


Fig. 6 TEM images of AuNPs capped with (A) DEQX and (B) OAQX synthesized at Au^{3+} /quinoxaline molar fractions of 1:0.2 and 1:1, respectively. Circularity analysis of (C) DEQX-capped AuNPs and (D) OAQX-capped AuNPs.

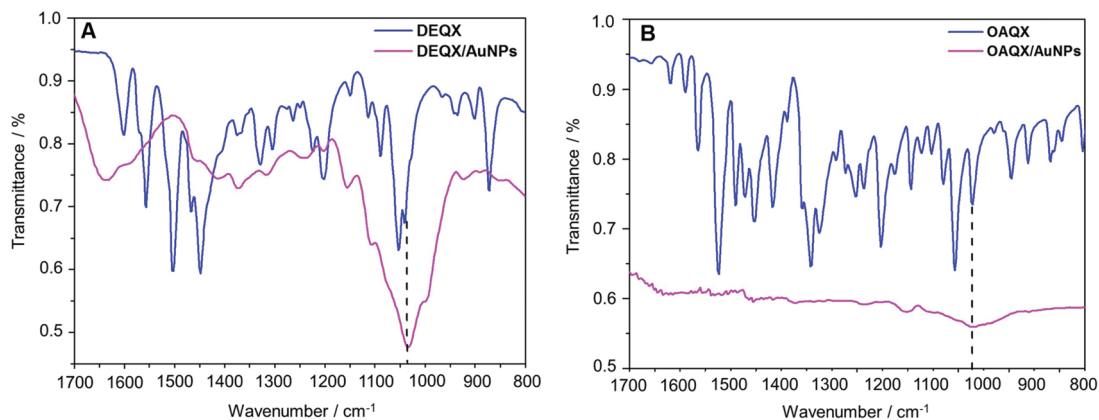


Fig. 7 FTIR in ATR mode of (A) DEQX-adsorbed AuNPs and (B) OAQX-adsorbed AuNPs. The spectra of the pure quinoxalines are also shown for comparison.

1:1, respectively. It is important to note that while the histogram of DEQX-stabilized AuNPs is centered at around 8.0 nm, the one related to OAQX-stabilized AuNPs is shifted to 11.5 nm, meaning that even at a lower concentration DEQX is more efficient than OAQX in delivering smaller nanoparticles. Fig. 6C and D depict circularity analysis of the AuNPs produced in this study. A circularity value of 1 means a perfectly symmetrical circle and values equal or below 0.90 denote non-spherical morphologies. While over 60% of AuNPs produced by either

quinoxaline were spherical in shape, slight differences in the proportion of non-spherical AuNPs were observed between samples. In the range 0.70–0.79, OAQX and DEQX delivered 20% and 8.7% of non-spherical nanoparticles, respectively. Therefore, not only is DEQX more efficient in delivering smaller nanoparticles, it provides more homogeneous ones in terms of morphology as well.

Fig. 7 presents FTIR spectra of DEQX, OAQX the respective quinoxaline-adsorbed AuNPs in ATR mode. Differences in the

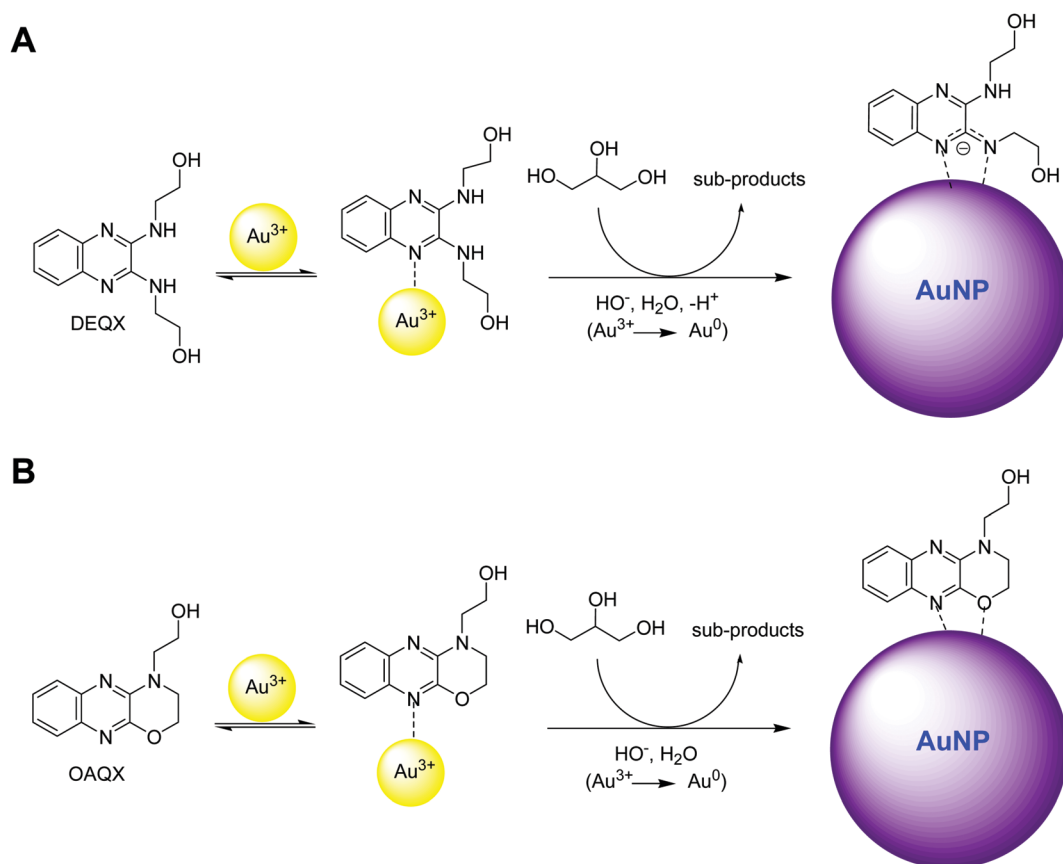


Fig. 8 Proposed mechanism for the formation of AuNPs with (A) DEQX and (B) OAQX.

range of 1450–1600 cm^{-1} , which is related to C=N, C=C and N–H bonds, suggest that DEQX (Fig. 7A) binds to the AuNPs surface through nitrogen atoms. The bands at 1039 cm^{-1} (C–O from alcohol) and 1053 cm^{-1} (C–N from amine) for pure DEQX become broader when the latter is adsorbed onto the AuNPs, suggesting that those functional groups are involved in the interaction with gold. In the case of OAQX (Fig. 7B), the spectrum for functionalized AuNPs is far less defined than that for DEQX-AuNPs. This might be an indicative that OAQX weakly binds to AuNPs and, therefore, is removed from the metallic surface during the centrifugation process. UV-vis and TEM results already showed that OAQX is less efficient than DEQX in stabilizing AuNPs. The general features for the spectrum are similar to the DEQX, including the region comprising C=N and C=C that becomes broader when OAQX is adsorbed onto AuNPs. Considerable alterations in bands associated to the ether group at 1056 cm^{-1} and 1203 cm^{-1} indicated that the oxygen of the saturated cycle also contributes to the interaction with the gold surface. For both quinoxaline-adsorbed AuNPs, the band at 1039 cm^{-1} and 1022 cm^{-1} for DEQX and OAQX, respectively, related to the alcoholic group remains at the same frequency, suggesting that it is not involved in the ligand-metal coordination. In both spectra, absorptions due to water bending at approximately 1635 cm^{-1} denote that AuNPs are hydrated to some extent.^{58,59}

3.4 Mechanism of AuNPs formation

In light of the results from UV-Vis and IR-ATR, we propose the following mechanism for the formation of AuNPs stabilized by the quinoxalines produced in the current study (Fig. 8): firstly, the quinoxaline derivatives bind to Au^{3+} generating a coordination complex that releases gold ions (quickly or slowly depending on the quinoxaline) which are then reduced by glycerol to form AuNPs. At this point, the strong alkaline medium induces deprotonation of DEQX, which, in turn, binds to the gold surface more strongly than OAQX since the anionic N=C–N[−] atomic arrangement of the former is more basic than the N=C–O system of the latter.

Molecular simulation studies have investigated the molecular interactions between peptides and Au-Pd nanoparticles⁶⁰ and the stabilization effect of organic molecules on Au nanoparticles.⁶¹ Heinz and coworkers⁶⁰ have demonstrated that short peptides (up to 12 residues) prefer to bind in vacant sites on fcc lattice of the Au surface molecules present structural/chemical requirements to bind preferably in vacant sites on Au fcc lattice at the {111} surface. Concerning the orientation of the molecule on the gold surface, for both systems, the binding of quinoxalines to the gold surface is more likely to take place perpendicularly, which is consistent with previously reports involving pyridine derivatives where vertical adsorption is more energetically favorable than flat adsorption.^{62,63}

4 Conclusion

We have shown that AuNPs can be easily functionalized with OAQX and DEQX, with the latter adsorbing more strongly onto

the nanoparticle surface. In addition, there is no need of employing a further stabilizing agent (e.g.: polymer) since both quinoxalines may act as stabilizers at appropriate concentrations. MD simulations indicated that DEQX and OAQX bind to PI3K α through a variety of amino-acid residues, a feature that makes those quinoxalines eligible to inhibit PI3K α enzymes. The combination of synthetic organic chemistry with nanoscience and MD simulations is an interesting approach to conceiving new potential platforms for cancer diagnostic and treatment.

Conflicts of interest

There are no conflicts to declare.

Acknowledgements

The authors gratefully acknowledge CNPq, FAPERN, CAPES and FINEP for the financial support of this work. This research was supported by High Performance Computing Center at NPAD/UFRN.

References

- 1 D. A. Wheeler and L. Wang, *Genome Res.*, 2013, **23**, 1054–1062.
- 2 R. T. Dorsam and J. S. Gutkind, *Nat. Rev. Cancer*, 2007, **7**, 79–94.
- 3 E. Tsanou, D. Peschos, A. Batistatou, A. Charalabopoulos and K. Charalabopoulos, *Anticancer Res.*, 2008, **28**, 3815–3826.
- 4 S. Kapitanović, T. Čačev, M. Antica, M. Kralj, G. Cavrić, K. Pavelić and R. Spaventi, *Exp. Mol. Pathol.*, 2006, **80**, 91–96.
- 5 F. E. Bleeker, S. Lamba, C. Zanon, R. J. Molenaar, T. J. M. Hulsebos, D. Troost, A. A. van Tilborg, W. P. Vandertop, S. Leenstra, C. J. F. van Noorden and A. Bardelli, *BMC Cancer*, 2014, **14**, 1–12.
- 6 F. E. Bleeker, R. J. Molenaar and S. Leenstra, *J. Neurooncol.*, 2012, **108**, 11–27.
- 7 P. J. Roberts and C. J. Der, *Oncogene*, 2007, **26**, 3291–3310.
- 8 L. M. Weiner, R. Surana and S. Wang, *Nat. Rev. Immunol.*, 2010, **10**, 317–327.
- 9 J. K. H. Liu, *Ann. Med. Surg.*, 2014, **3**, 113–116.
- 10 D.-F. Shi, T. D. Bradshaw, S. Wrigley, C. J. McCall, P. Lelieveld, I. Fichtner and M. F. G. Stevens, *J. Med. Chem.*, 1996, **39**, 3375–3384.
- 11 A. J. Hallett, B. M. Kariuki and S. J. A. Pope, *Dalton Trans.*, 2011, **40**, 9474–9481.
- 12 P. Marques-Gallego, M. A. Gamiz-Gonzalez, F. R. Fortea-Perez, M. Lutz, A. L. Spek, A. Pevec, B. Kozlevcar and J. Reedijk, *Dalton Trans.*, 2010, **39**, 5152–5158.
- 13 M. N. Noolvi, H. M. Patel, V. Bhardwaj and A. Chauhan, *Eur. J. Med. Chem.*, 2011, **46**, 2327–2346.
- 14 S.-H. Lee, N. Kim, S.-J. Kim, J. Song, Y.-D. Gong and S.-Y. Kim, *J. Cancer Res. Clin. Oncol.*, 2013, **139**, 1279–1294.

- 15 V. Desplat, M. Vincenzi, R. Lucas, S. Moreau, S. Savrimoutou, N. Pinaud, J. Lesbordes, E. Peyrilles, M. Marchivie, S. Routier, P. Sonnet, F. Rossi, L. Ronga and J. Guillon, *Eur. J. Med. Chem.*, 2016, **113**, 214–227.
- 16 T. R. Mielcke, A. Mascarello, E. Filippi-Chiela, R. F. Zanin, G. Lenz, P. C. Leal, L. D. Chirardia, R. A. Yunes, R. J. Nunes, A. M. O. Battastini, F. B. Morrone and M. M. Campos, *Eur. J. Med. Chem.*, 2012, **48**, 255–264.
- 17 S. I. Chiosea, J. R. Grandis, V. W. Y. Lui, B. Diergaard, J. H. Maxwell, R. L. Ferris, S. W. Kim, A. Luvison, M. Miller and M. N. Nikiforova, *BMC Cancer*, 2013, **13**, 1–7.
- 18 Y. Samuels, Z. Wang, A. Bardelli, N. Silliman, J. Ptak, S. Szabo, H. Yan, A. Gazdar, S. M. Powell, G. J. Riggins, J. K. V. Willson, S. Markowitz, K. W. Kinzler, B. Vogelstein and V. E. Velculescu, *Science*, 2004, **304**, 554.
- 19 P. Wu, Y. Su, X. Liu, B. Yang, Q. He and Y. Hu, *Bioorg. Med. Chem.*, 2012, **20**, 2837–2844.
- 20 P. Wu, Y. Su, X. Liu, L. Zhang, Y. Ye, J. Xu, S. Weng, Y. Li, T. Liu, S. Huang, B. Yang, Q. He and Y. Hu, *Eur. J. Med. Chem.*, 2011, **46**, 5540–5548.
- 21 A. M. Maley, Y. Terada, S. Onogi, K. J. Shea, Y. Miura and R. M. Corn, *J. Phys. Chem. C*, 2016, **120**, 16843–16849.
- 22 K. M. G. Lima, R. F. A. Junior, A. A. Araujo, A. L. C. S. L. Oliveira and L. H. S. Gasparotto, *Sens. Actuators, B*, 2014, **196**, 306–313.
- 23 I. N. Brigger, C. Dubernet and P. Couvreur, *Adv. Drug Delivery Rev.*, 2012, **64**(supplement), 24–36.
- 24 X. Huang, I. H. El-Sayed, W. Qian and M. A. El-Sayed, *J. Am. Chem. Soc.*, 2006, **128**, 2115–2120.
- 25 R. A. Sperling and W. J. Parak, *Philos. Trans. R. Soc., A*, 2010, **368**, 1333–1383.
- 26 M. C. Daniel and D. Astruc, *Chem. Rev.*, 2004, **104**, 293–346.
- 27 K. T. Savjani, A. K. Gajjar and J. K. Savjani, *ISRN Pharm.*, 2012, **2012**, 195727.
- 28 O. Trott and A. J. Olson, *J. Comput. Chem.*, 2010, **31**, 455–461.
- 29 D. Mandelker, S. B. Gabelli, O. Schmidt-Kittler, J. Zhu, I. Cheong, C.-H. Huang, K. W. Kinzler, B. Vogelstein and L. M. Amzel, *Proc. Natl. Acad. Sci. U. S. A.*, 2009, **106**, 16996–17001.
- 30 G. M. Morris, R. Huey, W. Lindstrom, M. F. Sanner, R. K. Belew, D. S. Goodsell and A. J. Olson, *J. Comput. Chem.*, 2009, **30**, 2785–2791.
- 31 M. D. Hanwell, D. E. Curtis, D. C. Lonie, T. Vandermeersch, E. Zurek and G. R. Hutchison, *J. Cheminf.*, 2012, **4**, 1–17.
- 32 Y. Duan, C. Wu, S. Chowdhury, M. C. Lee, G. Xiong, W. Zhang, R. Yang, P. Cieplak, R. Luo, T. Lee, J. Caldwell, J. Wang and P. Kollman, *J. Comput. Chem.*, 2003, **24**, 1999–2012.
- 33 C. I. Bayly, P. Cieplak, W. Cornell and P. A. Kollman, *J. Phys. Chem.*, 1993, **97**, 10269–10280.
- 34 G. Bussi, D. Donadio and M. Parrinello, *J. Chem. Phys.*, 2007, **126**, 014101.
- 35 B. Hess, H. Bekker, H. J. C. Berendsen and J. G. E. M. Fraaije, *J. Comput. Chem.*, 1997, **18**, 1463–1472.
- 36 S. Miyamoto and P. A. Kollman, *J. Comput. Chem.*, 1992, **13**, 952–962.
- 37 W. F. Van Gunsteren and H. J. C. Berendsen, *Mol. Simul.*, 1988, **1**, 173–185.
- 38 T. Darden, D. York and L. Pedersen, *J. Chem. Phys.*, 1993, **98**, 10089–10092.
- 39 G. Arfken, *Mathematical Methods for Physicists*, Academic Press, Orlando, FL, 3rd edn, 1985.
- 40 D. van der Spoel, P. J. van Maaren, P. Larsson and N. Timneanu, *J. Phys. Chem. B*, 2006, **110**, 4393–4398.
- 41 N. A. Baker, D. Sept, S. Joseph, M. J. Holst and J. A. McCammon, *Proc. Natl. Acad. Sci. U. S. A.*, 2001, **98**, 10037–10041.
- 42 W. Humphrey, A. Dalke and K. Schulten, *J. Mol. Graphics*, 1996, **14**(33–38), 27–38.
- 43 F. da Silva Miranda, A. M. Signori, J. Vicente, B. de Souza, J. P. Priebe, B. Szpoganicz, N. S. Gonçalves and A. Neves, *Tetrahedron*, 2008, **64**, 5410–5415.
- 44 D. E. Ames and M. I. Brohi, *J. Chem. Soc., Perkin Trans. 1*, 1980, 1384–1389.
- 45 C. A. Obafemi, W. Pfeleiderer and F. Taiwo, *Molbank*, 2006, **2006**, M508.
- 46 L. H. S. Gasparotto, A. C. Garcia, J. F. Gomes and G. Tremiliosi-Filho, *J. Power Sources*, 2012, **218**, 73–78.
- 47 A. G. Garcia, P. P. Lopes, J. F. Gomes, C. Pires, E. B. Ferreira, R. G. M. Lucena, L. H. S. Gasparotto and G. Tremiliosi-Filho, *New J. Chem.*, 2014, **38**, 2865–2873.
- 48 Z. A. Knight, B. Gonzalez, M. E. Feldman, E. R. Zunder, D. D. Goldenberg, O. Williams, R. Loewith, D. Stokoe, A. Balla, B. Toth, T. Balla, W. A. Weiss, R. L. Williams and K. M. Shokat, *Cell*, 2006, **125**, 733–747.
- 49 E. H. Walker, M. E. Pacold, O. Perisic, L. Stephens, P. T. Hawkins, M. P. Wymann and R. L. Williams, *Mol. Cell*, 2000, **6**, 909–919.
- 50 R. Marone, V. Cmiljanovic, B. Giese and M. P. Wymann, *Biochim. Biophys. Acta*, 2008, **1784**, 159–185.
- 51 K. Chen and L. Kurgan, *PLoS One*, 2009, **4**, e4473.
- 52 M. M. Heravi, S. Taheri, K. Bakhtiari and H. A. Oskooie, *Catal. Commun.*, 2007, **8**, 211–214.
- 53 J. F. Gomes, L. H. S. Gasparotto and G. Tremiliosi-Filho, *Phys. Chem. Chem. Phys.*, 2013, **15**, 10339–10349.
- 54 E. B. Ferreira, J. F. Gomes, G. Tremiliosi-Filho and L. H. S. Gasparotto, *Mater. Res. Bull.*, 2014, **55**, 131–136.
- 55 I. H. El-Sayed, X. Huang and M. A. El-Sayed, *Nano Lett.*, 2005, **5**, 829–834.
- 56 M. N. Khan, T. A. Khan, S. A. Al-Thabaiti and Z. Khan, *Spectrochim. Acta, Part A*, 2015, **149**, 889–897.
- 57 B. Đ. Glišić, B. Waržajtis, N. S. Radulović, U. Rychlewska and M. I. Djuran, *Polyhedron*, 2015, **87**, 208–214.
- 58 Á. I. López-Lorente, M. Sieger, M. Valcárcel and B. Mizaikoff, *Anal. Chem.*, 2014, **86**, 783–789.
- 59 J.-W. Park and J. S. Shumaker-Parry, *J. Am. Chem. Soc.*, 2014, **136**, 1907–1921.
- 60 H. H. Heinz, B. L. Farmer, R. B. Pandey, J. M. Slocik, S. S. Patnaik, R. Pachter and R. R. Naik, *J. Am. Chem. Soc.*, 2009, **131**, 9704–9714.
- 61 E. L. da Rocha, G. F. Caramori and C. R. Rambo, *Phys. Chem. Chem. Phys.*, 2013, **15**, 2282–2290.
- 62 K. Tonigold and A. Groß, *J. Chem. Phys.*, 2015, **132**, 224701.
- 63 V. J. Gandubert and B. Lennox, *Langmuir*, 2005, **21**, 6532.